J. Fluid Mech. (1987), *vol.* 184, *pp.* 335–356
Printed in Great Britain

Torsion effect on fully developed flow in a helical pipe

By HSIAO C. KAO
Lewis Research Center, Cleveland, OH 44135, USA

(Received 29 August 1986 and in revised form 10 February 1987)

Two approaches have been used to study the torsion effect on the fully developed laminar flow in a helical pipe of constant circular cross-section. The first approach is the series expansion method that perturbs the Poiseuille flow and is valid for low Dean numbers with both the dimensionless curvature and dimensionless torsion being much less than unity. The second is a numerical procedure that solves the complete Navier–Stokes equation and is applicable to intermediate values of the Dean number. The results obtained indicate that, as far as the secondary flow patterns are concerned, the presence of torsion can produce a large effect if the ratio of the curvature to the torsion is of order unity. In these cases the secondary flow, though still consisting of a pair of vortices, can be very much distorted. Under extreme conditions one vortex is so prevalent as to squeeze the second one into a narrow region. However, ordinarily the torsion effect is small and the secondary flow has the usual pattern of a pair of counter-rotating vortices of nearly equal strength. Concerning the flow resistance in the pipe the effect of torsion is always small in all the circumstances that have so far been considered.

1. Introduction

Although extensive studies have been made on flows in a toroidally curved pipe, comparatively little is known about the flows in a helical pipe. Even for a fully developed flow in the low-Reynolds-number regime, controversy exists. For instance, the recent papers by Wang (1981) and Germano (1982) reached different conclusions after analysing the problem. The former states that both curvature and torsion produce a first-order effect and the influence of torsion can be so dominant in some cases as to reduce the commonly occurring two-cell secondary flow to a single vortex, whereas the latter states that only curvature can cause the first-order effect and the effect of torsion is of second order.

In an attempt to settle these differences, we have re-examined this problem of a helical pipe using two different methods: the series expansion method, which is similar to the ones used by Wang and Germano; and the numerical computation of the complete Navier–Stokes equations.

The conclusion reached from the series expansion methods indicates that although torsion cannot produce a first-order effect, its presence can give rise to half-power terms, if an additional condition, that the order of magnitude of the dimensionless torsion λ is the same as that of the square root of the dimensionless curvature ϵ, is met. Under these conditions the leading term of torsion is of the $1\frac{1}{2}$ power of the perturbation parameter, which is the halfway between first and second order. If this condition is not imposed, the governing equations reduce to those given by Germano and the effect of torsion is relegated to second or higher order.

To complement the series expansion analysis and to investigate flows at moderately high Dean numbers, numerical computations of the full Navier–Stokes equations were also carried out. When the dimensionless curvature, which will be defined later, becomes relatively large, say $0.2 \leqslant \epsilon \leqslant 0.5$, the method of series expansion about the Poiseuille flow is no longer applicable even for small Dean numbers, and recourse to numerical calculations will have to be made. The results obtained in these cases for both small and moderately high Dean numbers seem to show that a small torsion may cause a significant change in the secondary flow pattern, and the aforementioned condition that $\lambda = O(2\epsilon)^{\frac{1}{2}}$ is no longer required. Furthermore, the change appears to be more pronounced as the Dean number becomes larger.

Although torsion can radically change the pattern of the secondary flow in a helical pipe, its influence on the volume flux ratio is relatively minor. For small values of the Dean number and based on the series expansion analysis, it is shown that the flux ratio remains unchanged compared with that of a curved pipe (Dean 1928) until the $2\frac{1}{2}$-power term. For an intermediate range of the Dean number, the numerical results obtained lend support to the suggestion made by Truesdell & Adler (1970) that the flux-ratio formula for a curved pipe is also applicable to a helical pipe if the curvature of the latter is used in place of that of a curved pipe. A similar conclusion was also reached by Murata *et al.* (1981), though they used somewhat simplified basic equations which assumed that the dimensionless curvature was small and the higher-order terms of curvature were neglected.

A comprehensive survey by Berger, Talbot & Yao (1983) on flow in curved pipes is now available, and so no mention will be made here of the available literature on previous work. However, after reading that survey, one is somewhat at a loss to discover that there are only four papers cited on the subject of helical pipes, notwithstanding their many applications, compared with over a hundred on toroidally curved pipes. We thus venture an attempt at an explanation.

Although a helical pipe involves an additional parameter compared with the curved pipe, which naturally increases its complexity, the main reason for the slow progress may stem from the need to use a non-orthogonal coordinate system for a helical pipe. The fact that the governing differential equations written in the non-orthogonal coordinates contain so many more terms than their counterparts in the orthogonal coordinates makes analysis or numerical calculation unwieldy and impedes progress considerably. Fortunately, this difficulty has been largely overcome by Germano, who introduced an ingenious transformation, rendering the governing differential equations for a helical pipe with circular cross-section expressible in orthogonal coordinates. The advantage is not only the simplification of the basic equations but also it makes the comparison with that of a curved pipe much clearer. Without this transformation, a rather severe approximation is needed to place an orthogonal coordinate system on a helical pipe. For instance, the requirement of a very small pitch in Manlapaz & Churchill (1980) accomplishes this purpose but at the same time reduces the problem to essentially that of a toroidally curved pipe.

The present study concerns steady laminar flow in a helical pipe of circular cross-section for small and intermediate values of the Dean number. Thus this paper is divided approximately into two parts. The first part is based on the method of series expansion applicable to small values of the Dean number along with the assumption that the pipe has only slight curvature and torsion. The second part deals with the numerical solution of the Navier–Stokes equations and is applicable to intermediate values of the Dean number. The flow is assumed to be fully developed.

2. Governing equations and formulation of the problem

The present coordinate system is that used by Germano (1982) and is depicted in figure 1. The centreline of a helical pipe is referred to as s' along which the unit tangent vector $\boldsymbol{T}$ is defined. The normal and binormal vectors are $\boldsymbol{N}$ and $\boldsymbol{B}$ respectively. A point E in the pipe is defined by a Cartesian position vector $\boldsymbol{R}$ which is a function of the local coordinate system (s', r', θ) and is given by

$$\boldsymbol{R} = \boldsymbol{R}_0(s') - r' \cos(\theta+\phi)\,\boldsymbol{N}(s') + r' \sin(\theta+\phi)\,\boldsymbol{B}(s'). \tag{1}$$

Note that this expression is somewhat different from that of Germano, because a right-handed helix is considered here instead of a left-handed one so that it reduces to the coordinate system adopted by McConalogue & Srivastava (1968) and others, when the torsion approaches zero.

Using the Serret–Frenet equations of a curve

$$\frac{\mathrm{d}\boldsymbol{T}}{\mathrm{d}s'} = \kappa\boldsymbol{N}, \quad \frac{\mathrm{d}\boldsymbol{N}}{\mathrm{d}s'} = \tau\boldsymbol{B} - \kappa\boldsymbol{T}, \quad \frac{\mathrm{d}\boldsymbol{B}}{\mathrm{d}s'} = -\tau\boldsymbol{N},$$

and the relationship

$$\boldsymbol{T} = \frac{\mathrm{d}\boldsymbol{R}_0}{\mathrm{d}s'}, \quad \boldsymbol{N} = \frac{1}{\kappa}\frac{\mathrm{d}\boldsymbol{T}}{\mathrm{d}s'}, \quad \boldsymbol{B} = \boldsymbol{T}\times\boldsymbol{N},$$

one can determine the metric of this system by first obtaining a total differential of the position vector

$$\mathrm{d}\boldsymbol{R} = \mathrm{d}s'[1+\kappa r' \cos(\theta+\phi)]\,\boldsymbol{T} + \mathrm{d}r'\boldsymbol{a}_r + r'\,\mathrm{d}\theta\,\boldsymbol{a}_\theta,$$

and then taking the scalar product

$$\mathrm{d}\boldsymbol{R}\cdot\mathrm{d}\boldsymbol{R} = [1+\kappa r' \cos(\theta+\phi)]^2\,\mathrm{d}s'^2 + \mathrm{d}r'^2 + r'^2\,\mathrm{d}\theta^2. \tag{2}$$

Here κ and τ are the curvature and torsion. $\boldsymbol{a}_r$ and $\boldsymbol{a}_\theta$ are two new vectors defined as follows:

$$\boldsymbol{a}_r = \sin(\theta+\phi)\,\boldsymbol{B} - \cos(\theta+\phi)\,\boldsymbol{N},$$

$$\boldsymbol{a}_\theta = \cos(\theta+\phi)\,\boldsymbol{B} + \sin(\theta+\phi)\,\boldsymbol{N},$$

to render the coordinate system orthogonal. In addition, the angle ϕ is defined as

$$\phi(s') = \int_{s_0'}^{s'} \tau(s)\,\mathrm{d}s_0'$$

and is therefore a function of s'. The lower limit s_0' is arbitrary as long as $s' \geqslant s_0'$.

With the orthogonal metric available, we can write the Navier–Stokes equations for a steady incompressible flow in the coordinates s', r', θ together with the geometric parameters κ, τ and ϕ as follows:

$$\omega\frac{\partial W}{\partial s'} + \frac{\partial U}{\partial r'} + \frac{U}{r'} + \frac{1}{r'}\frac{\partial V}{\partial\theta} + \kappa\omega[\cos(\theta+\phi)\,U - \sin(\theta+\phi)\,V] = 0, \tag{3}$$

$$\mathrm{D}W + \kappa\omega W[\cos(\theta+\phi)\,U - \sin(\theta+\phi)\,V] = -\omega\frac{\partial p}{\partial s'} + \nu\Big[\Big(\frac{1}{r'}+\frac{\partial}{\partial r'}\Big)$$

$$\times\Big(\frac{\partial W}{\partial r'} + \kappa\omega\cos(\theta+\phi)\,W - \omega\frac{\partial U}{\partial s'}\Big) + \frac{1}{r'}\frac{\partial}{\partial\theta}\Big(\frac{1}{r'}\frac{\partial W}{\partial\theta} - \kappa\omega\sin(\theta+\phi)\,W - \omega\frac{\partial V}{\partial s'}\Big)\Big], \tag{4}$$

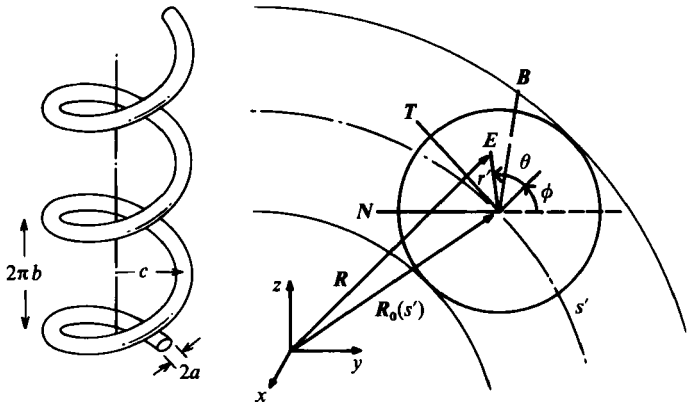

FIGURE 1. Depiction of a helical pipe and the coordinate system.

$$\mathrm{D}U-\frac{V^2}{r'}-\kappa\omega\cos(\theta+\phi)\,W^2=-\frac{\partial p}{\partial r'}+\nu\left[\left(\frac{1}{r'}\frac{\partial}{\partial\theta}-\kappa\omega\sin(\theta+\phi)\right)\right.$$
$$\left.\times\left(\frac{1}{r'}\frac{\partial U}{\partial\theta}-\frac{\partial V}{\partial r'}-\frac{V}{r'}\right)-\omega\frac{\partial}{\partial s'}\left(\frac{\partial W}{\partial r'}+\kappa\omega\cos(\theta+\phi)\,W-\omega\frac{\partial U}{\partial s'}\right)\right], \quad (5)$$

$$\mathrm{D}V+\frac{UV}{r'}+\kappa\omega\sin(\theta+\phi)\,W^2=-\frac{1}{r'}\frac{\partial p}{\partial\theta}+\nu\left[\omega\frac{\partial}{\partial s'}\left(\omega\frac{\partial V}{\partial s'}+\kappa\omega\sin(\theta+\phi)\,W-\frac{1}{r'}\frac{\partial W}{\partial\theta}\right)\right.$$
$$\left.-\left(\frac{\partial}{\partial r'}+\kappa\omega\cos(\theta+\phi)\right)\left(\frac{1}{r'}\frac{\partial U}{\partial\theta}-\frac{\partial V}{\partial r'}-\frac{V}{r'}\right)\right]. \quad (6)$$

In these expressions U, V and W are the velocity components in the $\boldsymbol{a}_r$, $\boldsymbol{a}_\theta$ and $\boldsymbol{T}$ directions respectively, and are functions of s', r', and $\theta+\phi$; p is the pressure, ν the kinematic viscosity, and D and ω are

$$\mathrm{D}=\omega W\frac{\partial}{\partial s'}+U\frac{\partial}{\partial r'}+\frac{V}{r'}\frac{\partial}{\partial\theta},\quad \omega=\frac{1}{1+\kappa r'\cos(\theta+\phi)}.$$

In a fully developed flow U, V, W are assumed to be independent explicitly of s' but they can still be dependent on it implicitly, as shown by Germano, through the relationship

$$\frac{\partial f(r',\theta+\phi)}{\partial s'}=\frac{\partial f}{\partial(\theta+\phi)}\frac{\partial(\theta+\phi)}{\partial s'}=\tau\frac{\partial f}{\partial(\theta+\phi)},$$

where f is an arbitrary function referring to the dependent variables. Furthermore, with the assumption of a fully developed flow and from (4) p can be written in the following form:

$$p=-\frac{G}{\rho}s'+p_2(r',\theta+\phi),$$

where G is a constant and ρ is the density of the fluid. This implies that the pressure gradient along the pipe centreline is now a constant (see, for example, McConalogue & Srivastava).

We now follow the usual steps to eliminate the pressure terms in (5) and (6) by

cross-differentiation, and at the same time define the Dean number D and the following dimensionless variables:

$$\left.\begin{gathered} r=\frac{r'}{a}, \quad \epsilon=a\kappa, \quad \lambda=a\tau, \quad u=\frac{a}{\nu}U, \quad v=\frac{a}{\nu}V, \\ w=\frac{(2\kappa a^3)^{\frac{1}{2}}}{\nu}W, \quad \frac{\partial p}{\partial s'}=-\frac{G}{p}+\tau\frac{\partial p_2}{\partial(\theta+\phi)}, \quad D=\frac{Ga^2}{\mu}\left(\frac{2\kappa a^3}{\nu^2}\right)^{\frac{1}{2}}, \\ \frac{\partial}{\partial\theta}p_2(r',\theta+\phi)=\frac{\partial}{\partial(\theta+\phi)}p_2(r',\theta+\phi), \quad \Omega=\frac{\partial v}{\partial r}+\frac{v}{r}-\frac{1}{r}\frac{\partial u}{\partial(\theta+\phi)}. \end{gathered}\right\} \tag{7}$$

Here the equality for p_2 in the last line is merely an example and holds true for other dependent variables. a refers to the radius of the pipe, and Ω is the dimensionless vorticity for the secondary flow and appears as the dependent variable in the vorticity transport equation.

The necessary differential equations for the problem are now available and are shown in Appendix A. To solve the problem, we impose the no-slip condition at the pipe wall

$$u=v=w=0 \quad \text{at } r=1, \tag{8}$$

or the equivalent condition for the vorticity, together with the requirement that all flow quantities are regular at $r=0$.

3. Series expansions for small-Dean-number flows

The governing equations shown in Appendix A can be substantially simplified, as shown in the following, if it is assumed that u, v and w are of the same order of magnitude, and $\epsilon \ll 1$, $\lambda \ll 1$, and $\lambda/(2\epsilon)^{\frac{1}{2}}=O(1)$:†

$$\frac{\partial v}{\partial\alpha}+\frac{\partial}{\partial r}(ru)+\beta^{\frac{1}{2}}r\frac{\partial w}{\partial\alpha}=0, \tag{9}$$

$$\nabla^2 w-u\frac{\partial w}{\partial r}-\frac{v}{r}\frac{\partial w}{\partial\alpha}=-D+\beta^{\frac{1}{2}}w\frac{\partial w}{\partial\alpha}, \tag{10}$$

$$\begin{aligned} \nabla^2\Omega-\frac{1}{r}u\Omega-\frac{\partial}{\partial r}(u\Omega)-\frac{1}{r}\frac{\partial}{\partial\alpha}(v\Omega) \\ =w\left(\sin\alpha\frac{\partial w}{\partial r}+\frac{1}{r}\cos\alpha\frac{\partial w}{\partial\alpha}\right)+\beta^{\frac{1}{2}}\left(w\frac{\partial\Omega}{\partial\alpha}-\frac{1}{r}\frac{\partial w}{\partial\alpha}\frac{\partial u}{\partial\alpha}+\frac{\partial w}{\partial r}\frac{\partial v}{\partial\alpha}\right), \end{aligned} \tag{11}$$

where $\alpha=\theta+\phi$, $\beta^{\frac{1}{2}}=\lambda/(2\epsilon)^{\frac{1}{2}}$ and

$$\nabla^2=\frac{\partial^2}{\partial r^2}+\frac{1}{r}\frac{\partial}{\partial r}+\frac{1}{r^2}\frac{\partial^2}{\partial\alpha^2}.$$

Equations (9)–(11) are the continuity, the axial momentum and the vorticity transport equations respectively. This system shows that even for a loosely coiled pipe with both ϵ and λ much less than unity the effect of pitch (torsion) on the pipe

† The assumption that these velocity components are of the same order of magnitude holds generally true for the intermediate range of the Dean numbers. At low Dean numbers u and v are usually much smaller than w. This diminution in magnitude of u and v does not, however, invalidate the approximation.

flow need not be negligible as long as the ratio $\beta^{\frac{1}{2}}$ remains finite. However, if the condition that $\beta^{\frac{1}{2}} = O(1)$ is dropped and $\beta^{\frac{1}{2}} \ll 1$, (9)–(11) reduce to Dean's classical form as was shown in Germano (1982). In this case torsion can only exert a second-order effect on flows in a helical pipe.

We now solve (9)–(11) together with the boundary condition (8) by means of a series expansion method. Before doing this it is convenient to convert the present dimensionless quantities to those given by Dean, so that a direct comparison can be made. The relationship is very simple and is given by

$$u = \bar{u}, \quad v = \bar{v}, \quad w = \tfrac{1}{4}D\bar{w}, \quad \Omega = \bar{\Omega}, \quad \tfrac{1}{4}D = K^{\frac{1}{2}},$$

where the quantities with bars denote Dean's variables, and K is the original Dean number defined by Dean. With these new variables, (9)–(11) assume the form

$$\frac{\partial v}{\partial \alpha} + \frac{\partial}{\partial r}(ru) = -\beta^{\frac{1}{2}} K^{\frac{1}{2}} r \frac{\partial \bar{w}}{\partial \alpha}, \tag{12}$$

$$\nabla^2 \bar{w} - \left(u\frac{\partial \bar{w}}{\partial r} + \frac{v}{r}\frac{\partial \bar{w}}{\partial \alpha}\right) = -4 + \beta^{\frac{1}{2}} K^{\frac{1}{2}} \bar{w} \frac{\partial \bar{w}}{\partial \alpha}, \tag{13}$$

$$\begin{aligned} \nabla^2 \Omega - \left(u\frac{\partial \Omega}{\partial r} + \frac{v}{r}\frac{\partial \Omega}{\partial \alpha}\right) &= K\bar{w}\left(\sin\alpha \frac{\partial \bar{w}}{\partial r} + \frac{\cos\alpha}{r}\frac{\partial \bar{w}}{\partial \alpha}\right) \\ &\quad + \beta^{\frac{1}{2}} K^{\frac{1}{2}}\left(\bar{w}\frac{\partial \Omega}{\partial \alpha} - \Omega\frac{\partial \bar{w}}{\partial \alpha}\right) - \beta^{\frac{1}{2}} K^{\frac{1}{2}}\left(\frac{1}{r}\frac{\partial \bar{w}}{\partial \alpha}\frac{\partial u}{\partial \alpha} - \frac{\partial \bar{w}}{\partial r}\frac{\partial v}{\partial \alpha}\right), \end{aligned} \tag{14}$$

where the bars over u, v and Ω have been dropped, since these variables are the same.

Upon introduction of a modified stream function ψ to replace the continuity equation (12), which is similar to the one used by Hamed & Abdallah (1979),

$$\left.\begin{aligned} u &= \frac{1}{r}\frac{\partial \psi}{\partial \alpha} - \beta^{\frac{1}{2}} K^{\frac{1}{2}} \frac{1}{r}\int_0^r r \frac{\partial \bar{w}}{\partial \alpha}\,\mathrm{d}r, \\ v &= -\frac{\partial \psi}{\partial r}, \end{aligned}\right\} \tag{15}$$

this system reduces to (16) and (17) as shown below. They bear close resemblance to those of Dean and become Dean's equation if $\beta = 0$.

$$\nabla^2 \bar{w} + 4 = \frac{1}{r}\left(\frac{\partial \psi}{\partial \alpha}\frac{\partial \bar{w}}{\partial r} - \frac{\partial \psi}{\partial r}\frac{\partial \bar{w}}{\partial \alpha}\right) + \beta^{\frac{1}{2}} K^{\frac{1}{2}}\left(\bar{w}\frac{\partial \bar{w}}{\partial \alpha} - \frac{1}{r}\frac{\partial \bar{w}}{\partial r}\int_0^r r\frac{\partial \bar{w}}{\partial \alpha}\,\mathrm{d}r\right), \tag{16}$$

$$\begin{aligned} \nabla^4 \psi &= \frac{1}{r}\left(\frac{\partial \psi}{\partial \alpha}\frac{\partial}{\partial r} - \frac{\partial \psi}{\partial r}\frac{\partial}{\partial \alpha}\right)\nabla^2 \psi + \beta^{\frac{1}{2}} K^{\frac{1}{2}}\left[\frac{1}{r^4}\int_0^r r\left(4\frac{\partial^2 \bar{w}}{\partial \alpha^2} + \frac{\partial^4 \bar{w}}{\partial \alpha^4}\right)\mathrm{d}r\right. \\ &\quad + \frac{2}{r^4}\frac{\partial \psi}{\partial \alpha}\int_0^r r\frac{\partial^2 \bar{w}}{\partial \alpha^2}\,\mathrm{d}r + \frac{1}{r^3}\frac{\partial \psi}{\partial r}\int_0^r r\frac{\partial^3 \bar{w}}{\partial \alpha^3}\,\mathrm{d}r - \frac{1}{r}\frac{\partial}{\partial r}\nabla^2 \psi \int_0^r r\frac{\partial \bar{w}}{\partial \alpha}\,\mathrm{d}r\Big] \\ &\quad + \beta^{\frac{1}{2}} K^{\frac{1}{2}}\left[\frac{1}{r}\frac{\partial^3 \bar{w}}{\partial r\,\partial \alpha^2} - \frac{1}{r^2}\left(2 + \frac{\partial \psi}{\partial \alpha}\right)\frac{\partial^2 \bar{w}}{\partial \alpha^2} - \left(\frac{\partial \bar{w}}{\partial \alpha} - \bar{w}\frac{\partial}{\partial \alpha}\right)\nabla^2 \psi + \frac{1}{r^2}\frac{\partial \bar{w}}{\partial \alpha}\frac{\partial^2 \psi}{\partial \alpha^2} + \frac{\partial \bar{w}}{\partial r}\frac{\partial^2 \psi}{\partial r\,\partial \alpha}\right] \\ &\quad + K\left[-\bar{w}\left(\sin\alpha\frac{\partial \bar{w}}{\partial r} + \frac{\cos\alpha}{r}\frac{\partial \bar{w}}{\partial \alpha}\right) + \frac{\beta}{r^2}\int_0^r r\frac{\partial \bar{w}}{\partial \alpha}\,\mathrm{d}r\left(\frac{\partial^2 \bar{w}}{\partial \alpha^2} - \frac{2}{r^2}\int_0^r r\frac{\partial^2 \bar{w}}{\partial \alpha^2}\,\mathrm{d}r\right)\right. \\ &\quad \left.\left. - \frac{\beta}{r^2}\bar{w}\int_0^r r\frac{\partial^3 \bar{w}}{\partial \alpha^3}\,\mathrm{d}r\right]. \end{aligned} \tag{17}$$

The boundary conditions for these equations are

$$\overline{w} = 0, \quad \frac{\partial \psi}{\partial r} = 0, \quad \psi = \beta^{\frac{1}{2}} K^{\frac{1}{2}} \int_0^{\alpha} \int_0^1 r \frac{\partial \overline{w}}{\partial \alpha} \mathrm{d}r \, \mathrm{d}\alpha \quad \text{at } r = 1, \tag{18}$$

along with the condition that ψ and $\overline{w}$ are regular at $r = 0$. Note that the angle α is still equal to $\theta + \phi$. However, in a fully developed flow ϕ is arbitrary and can be regarded as zero.

This system is solved for small values of the Dean number K by expanding the dependent variables in powers of K:

$$\left.\begin{aligned} \overline{w} &= w_0 + K w_1 + K^{\frac{3}{2}} w_2 + K^2 w_3 + K^{\frac{5}{2}} w_4 + \ldots, \\ \psi &= \psi_0 + K \psi_1 + K^{\frac{3}{2}} \psi_2 + K^2 \psi_3 + K^{\frac{5}{2}} \psi_4 + \ldots. \end{aligned}\right\} \tag{19}$$

The appearance of the half-power terms here is the consequence of the non-zero β in (16) and (17).

As usual, the leading terms for w and ψ are the straight-pipe Poiseuille flow solutions that are

$$\psi_0 = 0, \quad w_0 = 1 - r^2.$$

The first-order terms can then be solved, which are

$$\psi_1 = \tfrac{1}{144}(r - \tfrac{9}{4}r^3 + \tfrac{3}{2}r^5 - \tfrac{1}{4}r^7) \sin\alpha,$$

$$w_1 = \tfrac{1}{576}(\tfrac{19}{40}r - r^3 + \tfrac{3}{4}r^5 - \tfrac{1}{4}r^7 + \tfrac{1}{40}r^9) \cos\alpha.$$

Up to this order, solutions are identical with Dean's. In order to see the effect of the pitch, we carry out the solutions to the order of $K^{\frac{3}{2}}$ in detail. For this the governing differential equations are

$$\nabla^2 w_2 = \frac{1}{r} \frac{\partial \psi_2}{\partial \alpha} \frac{\partial w_0}{\partial r} + \beta^{\frac{1}{2}} \left(w_0 \frac{\partial w_1}{\partial \alpha} - \frac{1}{r} \frac{\partial w_0}{\partial r} \int_0^r r \frac{\partial w_1}{\partial \alpha} \mathrm{d}r \right), \tag{20}$$

$$\nabla^4 \psi_2 = \beta^{\frac{1}{2}} \left(\frac{4}{r^4} \int_0^r r \frac{\partial^2 w_1}{\partial \alpha^2} \mathrm{d}r + \frac{1}{r^4} \int_0^r r \frac{\partial^4 w_1}{\partial \alpha^4} \mathrm{d}r + \frac{1}{r} \frac{\partial^3 w_1}{\partial r \, \partial \alpha^2} - \frac{2}{r^2} \frac{\partial^2 w_1}{\partial \alpha^2} + w_0 \frac{\partial}{\partial \alpha} \nabla^2 \psi_1 + \frac{\partial w_0}{\partial r} \frac{\partial^2 \psi_1}{\partial r \, \partial \alpha} \right). \tag{21}$$

The boundary conditions for this system at $r = 1$ are

$$w_2 = 0, \quad \frac{\partial \psi_2}{\partial r} = 0,$$

$$\psi_2 = \beta^{\frac{1}{2}} \int_0^{\alpha} \int_0^1 r \frac{\partial w_1}{\partial \alpha} \mathrm{d}r \, \mathrm{d}\alpha = \frac{\beta^{\frac{1}{2}}}{4 \times 144} \frac{277}{7 \times 990} \cos\alpha.$$

The solutions to (20) and (21) are straightforward and assume the form

$$\psi_2 = \frac{\beta^{\frac{1}{2}}}{4 \times 576} (-\tfrac{13}{60}r + \tfrac{79}{60}r^3 - \tfrac{49}{30}r^5 + \tfrac{13}{14}r^7 - \tfrac{47}{180}r^9 + \tfrac{17}{660}r^{11}) \cos\alpha, \tag{22}$$

$$w_2 = \frac{\beta^{\frac{1}{2}}}{4 \times 576} (\tfrac{17\,656}{22\,5225}r + \tfrac{13}{90}r^2 - \tfrac{79}{150}r^4 + \tfrac{7}{15}r^6 - \tfrac{13}{63}r^8 + \tfrac{47}{990}r^{10} - \tfrac{17}{4290}r^{12})$$

$$\times \cos\alpha + \frac{\beta^{\frac{1}{2}}}{4 \times 576} (\tfrac{14\,789}{11\,8800}r - \tfrac{19}{80}r^3 + \tfrac{139}{720}r^5 - \tfrac{9}{80}r^7 + \tfrac{11}{280}r^9 - \tfrac{79}{10\,800}r^{11} + \tfrac{3}{6160}r^{13}) \sin\alpha. \tag{23}$$

It is evident from these solutions that although the appearance of $O(K^{\frac{3}{2}})$-terms makes no contribution to the flow rate to this order, the distribution of the axial

velocity component w and the secondary flow patterns will be different from those of a curved pipe. In particular, the patterns will no longer be symmetrical.

This process of solving higher-order terms presents no difficulty and can continue, except that it becomes increasingly laborious. Solutions for ψ_3 and w_3 have also been obtained and are shown in Appendix B.

Turning our attention now to the global property of a helical pipe, we define the volume-flux ratio as

$$\frac{Q}{Q_S} = \frac{2}{\pi}\int_0^{2\pi}\int_0^1 \overline{w} r \, dr \, d\alpha,$$

where Q denotes the flux in a helical pipe and Q_S the flux in a straight pipe for the same pressure gradient as that in a helical pipe. It turns out that the expression for the flux ratio to the order of K^2 is identical with that for a curved pipe. Thus, to this order torsion does not affect the flow rate in a helical pipe. This is in agreement with the conclusion reached by Wang (1981). We thus have to obtain the next approximation in (19) in order to see the influence of torsion. This may be done without solving w_4 completely, since only the part of the solution that does not involve the trigonometric functions makes a contribution to the flux. After this process is carried out, the ratio becomes

$$\frac{Q}{Q_S} = 1 - 0.03058\left(\frac{K}{576}\right)^2 - 0.06816\,\beta^{\frac{1}{2}}\left(\frac{K}{576}\right)^{\frac{5}{2}} + \ldots. \tag{24}$$

As is seen, the first two terms are the same as those given by Dean, which are for a curved pipe. The third term contains the parameter β, which brings in the effect of torsion.

Previous investigations show that the series solution of the flow rate for a curved pipe is valid for $K \leqslant 576$ ($D \leqslant 96$). Since the coefficient in the third term of (24) is somewhat larger than that in the preceding term, the radius of convergence may be considerably smaller than that of a curved pipe. The anomaly in figure 2(*a*) to be stated later may actually reflect this property. The question of convergence cannot, however, be answered here because of an insufficient number of terms. Extension to higher-order terms by computer, similar to what was done by Larrain & Bonilla (1970) or Van Dyke (1978), should be possible. When this is done, the range of convergence may be examined. However, comparison of solutions to (24) with those by numerical calculations seems to indicate that the range of applicability of (24) is still approximately $K \leqslant 576$.

4. Graphic illustration and discussion of series solution

The secondary streamlines and the axial velocity patterns for laminar flows in a toroidally curved pipe are all symmetric with respect to the central plane. The presence of torsion in a helical pipe makes these patterns asymmetric, beginning with terms of $O(K^{\frac{3}{2}})$. Therefore, it is assumed that the degree of asymmetry in the secondary flow patterns reveals directly the extent of the torsion effect.

The customary method of displaying the secondary flow patterns is to plot the secondary streamlines. This method is, however, not convenient here, since the stream function defined in (15) is not a true stream function. Instead, the resultants of u, v velocity components at the pipe cross-sections are shown. These represent then the projected velocity vectors or the cross-flow vectors.

In order to facilitate discussion we present here not only the secondary flow

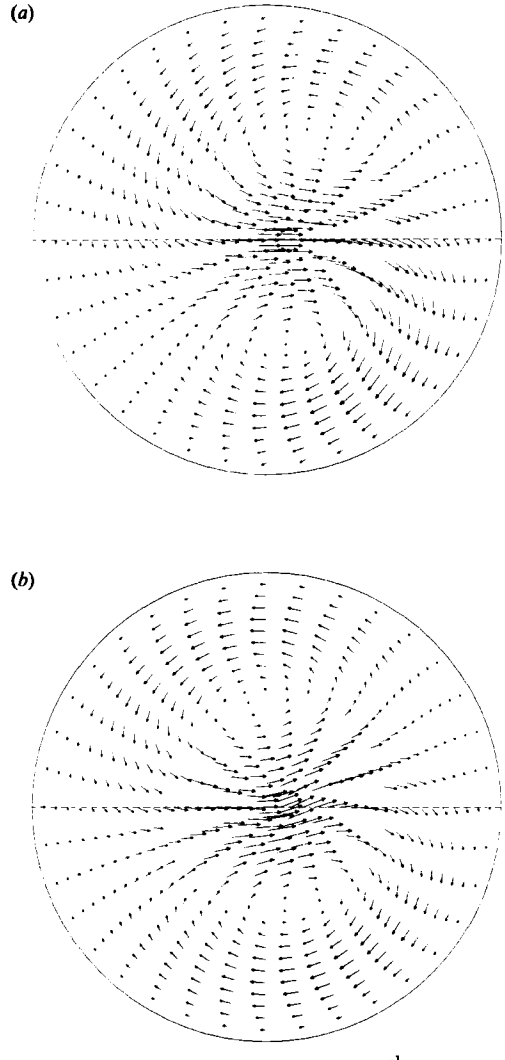

FIGURE 2. Vector plot of the secondary flow. (*a*) $D = 80$, $\beta^2 = 0.5$ (series solution). (*b*) $D = 80$, $\epsilon = 0.005$, $\lambda = 0.05$, $\beta^2 = 0.5$ (numerical solution).

patterns from the series expansion but also those obtained by a numerical method, which will be discussed in more detail later.

Shown in figure 2(*a*) are the cross-flow vectors based on the solutions of (19). These vectors are stretched or reduced by an arbitrary constant so that pictures are legible and details are not masked. The relative magnitude is, of course, unaltered. This technique is also used for every velocity–vector plot hereafter.

At first glance it appears that the series solution in figure 2(*a*) is in error, since there is an inflow to the lower half but no outflow from there. However, since this is not exactly a convergent solution some local anomaly may be expected. To ascertain that this is the case, another cross-flow vector plot is included, figure 2(*b*), which is obtained numerically under similar conditions, with $\epsilon = 0.005$, and $\lambda = 0.05$ to meet the requirement that $\epsilon \ll 1$ and $\lambda \ll 1$. It is seen by overlaying these two figures that the velocity vectors fall almost on top of each other except in the area near the centre,

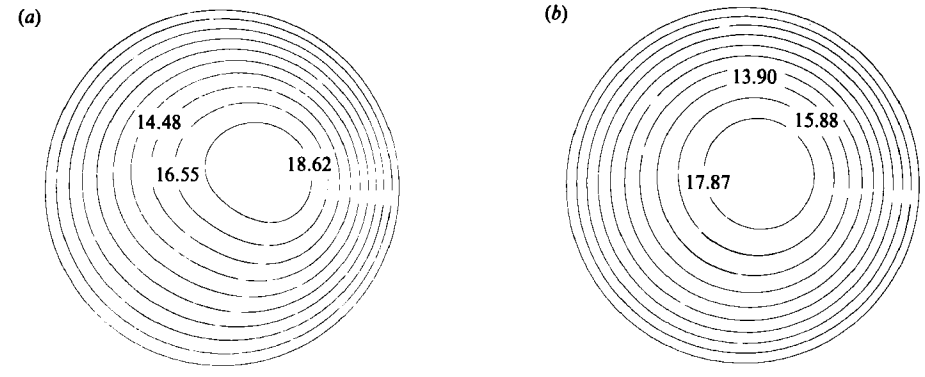

FIGURE 3. Contour lines of the streamwise velocity component corresponding to the two cases in figure 2. (The indicated values are the dimensionless quantity w defined in (7).) (*a*) $D = 80$, $\beta^{\frac{1}{2}} = 0.5$ series solution. (*b*) $D = 80$, $\epsilon = 0.005$, $\lambda = 0.05$, $\beta^{\frac{1}{2}} = 0.5$ (numerical solution).

where the anomaly of the series solution occurs. The numerical solution displays upward velocity vectors near the centre, which provide the outflow needed for the lower half. In addition, the dividing line between the two counter-rotating vortices in figure 2(*b*) appears to have rotated approximately 25° upward compared with that in a curved pipe, which is the dotted line on the central plane. If the main flow in a helical pipe moves in the clockwise direction about the axis of the helix coil, as opposed to the counterclockwise here, this dividing line is expected to be shifted downward.

Accompanying the cross-flow plots are the axial velocity contour lines plotted in figure 3(*a*, *b*). These are obtained under the same conditions as in figure 2. As seen, these patterns are also asymmetric with the peak velocities shifted north-eastward, though the shift in the numerical solution is less pronounced. This implies that the secondary flow in a helical pipe transports the fluid particles both away from the inner wall and upward if the main flow moves in the counterclockwise direction.

Next we show in figures 4 and 5 two cross-flow plots to demonstrate that as β decreases the asymmetry of the flow pattern diminishes (figure 4), and that the secondary flow for $D \leqslant 30$ is always nearly symmetric if β is less than unity (figure 5). Note that although these two plots are based on the solutions of (19), two numerical calculations were also performed to check their accuracy by fixing ϵ to be 0.05 and adjusting λ to make the β equal to those in figures 4 and 5. The results were found to agree fairly well with those from (19), except for the central anomaly. Thus there is incomplete agreement between the series and numerical solutions even at a Dean number as low as 30.

The remarks that a small β or a small D results in a nearly symmetric profile are only valid under the conditions that $\epsilon \ll 1$ and $\lambda \ll 1$. If ϵ is not small, neither of these statements holds. To confirm these claims, two additional figures, 6 and 7, are included. These are the profiles from two numerical calculations choosing an intermediate value of ϵ, corresponding to $\beta = 0.0067$ and 0.168. Although these β are much smaller than those in figures 4 and 5, the secondary-flow profiles are still fairly asymmetric. This seems to imply that the importance of torsion is greatly enhanced by the curvature and its nonlinear interactions.

We now examine the flux ratio in helical pipes with moderately high dimensionless curvatures. It is found that the previous conclusion of a higher-order effect of torsion

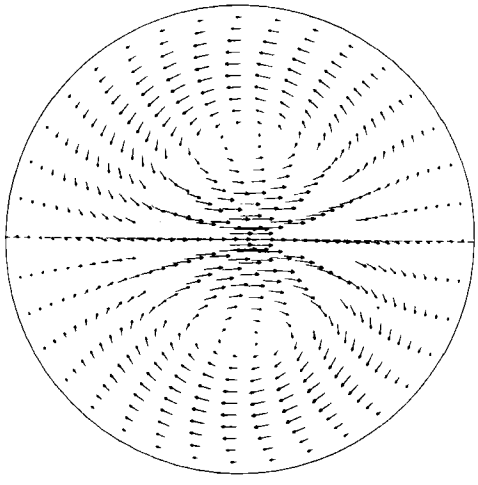

FIGURE 4. Vector plot of the secondary flow at $D = 80$, $\beta^{\frac{1}{2}} = 0.25$ (series solution).

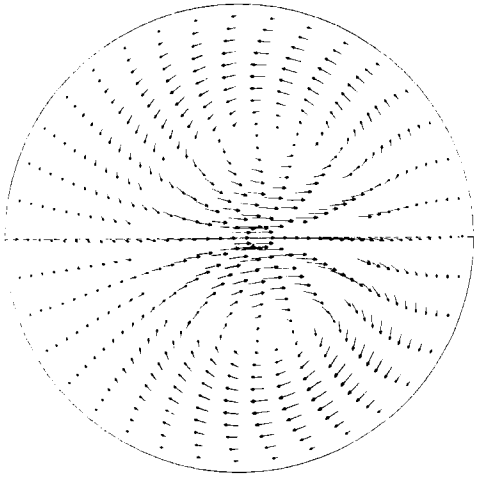

FIGURE 5. Vector plot of the secondary flow at $D = 30$, $\beta^{\frac{1}{2}} = 0.5$ (series solution).

is still valid. To demonstrate this point, we quote the computed flux ratios obtained from two numerical runs:

$$\frac{Q}{Q_S} = 0.9827 \quad \text{with } D = 80, \quad \epsilon = 0.4, \quad \lambda = 0 \text{ (curved pipe)};$$

$$\frac{Q}{Q_S} = 0.9978 \quad \text{with } D = 80, \quad \epsilon = 0.4, \quad \lambda = 0.25 \text{ (helical pipe)}.$$

Note that the flux ratio in a helical pipe is somewhat larger than the flux ratio in a curved pipe for the same Dean number. This seems to be true in general irrespective of the Dean number and curvature; examples will also be given later for moderately high-Dean-number cases to demonstrate this property. Thus, it follows that for the same curvature and Dean number the effect of the torsion is to reduce the resistance

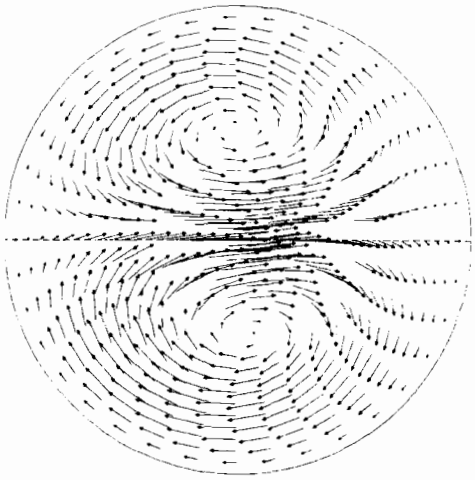

FIGURE 6. Vector plot of the secondary flow at $D = 80$, $\epsilon = 0.4$, $\lambda = 0.06$, $\beta = 0.0067$ (numerical solution).

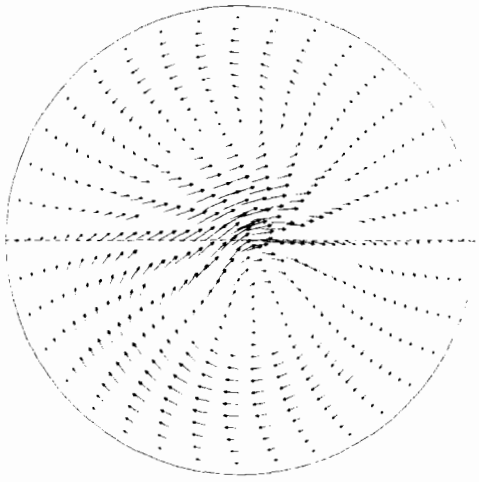

FIGURE 7. Vector plot of the secondary flow at $D = 30$, $\epsilon = 0.4$, $\lambda = 0.15$, $\beta = 0.168$ (numerical solution).

in the pipe. For very small Dean numbers, the resistance in a curved pipe can actually be less than that in a straight pipe (Larrain & Bonilla 1970). If the torsion effect is added to the problem, this cross-over point will perhaps occur sooner.

The many numerical examples obtained by integrating the full Navier–Stokes equations for small Dean numbers from small to moderately large curvatures, seem to reveal the property that the position of the peak axial velocity component is influenced more by the curvature than by the torsion. For instance, when the curvature is small, its position is generally in the north-eastern quadrant. However, as the curvature increases, it moves gradually to the west and may end up in the north-western quadrant as shown in figure 8.

The configuration shown in Wang's (1981) paper, in which a pair of vortices eventually evolve to a single vortex as the torsion parameter increases, has not been

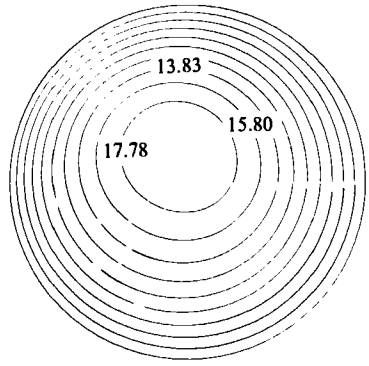

FIGURE 8. Contour lines of streamwise velocity component at $D = 80$, $\epsilon = 0.4$, $\lambda = 0.25$ (numerical solution).

found here for small Dean numbers. It is not certain whether this would happen in the range of intermediate Dean numbers. However, in the latter case one vortex can appear substantially smaller than the other, as will be shown later.

5. Finite-difference procedures for intermediate Dean numbers

For intermediate Dean numbers it is necessary to solve the problem numerically. The governing differential equations are the full Navier–Stokes equations, (A 2)–(A 4) in Appendix A. The resulting governing equations, though more complicated, are similar to (16) and (17), except that the vorticity Ω is retained as a dependent variable instead of the modified stream function in (17).

Finite-difference numerical solutions were carried out by using the power-law scheme of Patankar (1979); however, the method of quadratic upstream differencing (QUICK) of Leonard (1979) was also used for some of the solutions to compare the relative accuracy of these two methods. The computational procedure for the latter method was essentially that of Han, Humphrey & Launder (1981) with some changes made to achieve the stability needed. Since these procedures are established and well documented, no details are necessary here. It suffices to say that all calculations were implemented on a uniformly spaced grid system, covering the computational domain of a unit circle. The resulting finite-difference equations are solved by the line relaxation method with an under-relaxation factor and by sweeping in the increasing angular direction. The sequence of calculation in one iteration cycle is to solve (A 4) first and then (A 2) and (A 3), always using the most recent approximation to a variable. This process is repeated until the changes in two consecutive iterations for every dependent variable are less than the specified tolerance criteria.

Equations (A 2)–(A 4) are valid for $r > 0$. The singularity at $r = 0$ is caused by the particular choice of the coordinate system and can be removed by recasting the equations locally into Cartesian coordinates. At first glance this process does not seem to be optimum, since there are better techniques available to deal with this singularity (see, example, Soh & Berger 1984). However, in most cases a special treatment is still needed at $r = 0$, which calls for an average of flow quantities at $r = 0$. Writing the governing equation into a finite-difference form at $r=0$ in terms of the local Cartesian coordinates may then be viewed as an alternative method of obtaining these averaged quantities.

Before carrying out calculations for various conditions, we tested computational accuracy by comparing results predicted by the power-law method with those by QUICK and by making a grid-refinement study based on the former method.

Since the power-law method is essentially a first-order upwind scheme, it is liable to false diffusion when streamlines are oblique to grid lines. However, secondary streamlines are mostly aligned with the grid lines (except in the region where the two streams converge or diverge strongly), and the effect of false diffusion is not expected to be large. To substantiate this conjecture, we used the QUICK method since it is known that this method – though less stable – can reduce false diffusion. Several solutions were then obtained by both methods and comparisons were made. For the cases computed with $D \leqslant 2000$, the difference was found to be small.

A grid-refinement study was next carried out to determine an adequate grid distribution for the problem. The number of grid points in the radial direction of a unit circle was increased from 21 to 41 and finally to 81 points. As the Dean number increases, the variation of flow properties near the pipe surface also increases and the grid spacing in the radial direction has to be decreased accordingly. In order to show the difference between a coarse and a fine grid, a numerical comparison is given here. This is done by utilizing the root-mean-square residuals (RMSR) formula for the secondary-flow stream functions in a curved pipe with $D = 2000$ and $\epsilon = 0.2$:

$$\text{RMSR} = \left(\sum_{i,j}^{M,N} \left(\frac{\psi_{ij} - \psi'_{ij}}{\psi'_{ij}} \right)^2 \Big/ (M-1)(N-1) \right)^{\frac{1}{2}},$$

where ψ_{ij} is the secondary-flow stream function with a grid distribution of either 21×72 or 41×72 points, and ψ'_{ij} is that with a grid distribution of 81×72 points. Since we compare only these quantities at points of the coarsest grid, M and N are equal to 21 and 72 respectively. The results obtained are 0.0520 between grids of 21×72 and 81×72 points, and 0.0144 between those of 41×72 and 81×72 points. In view of the relatively small difference in the second case, a grid spacing of 41×72 points was selected for calculations for the intermediate Dean numbers and 21×72 points otherwise. No investigation was, however, made for selecting grid spacing in the angular direction, since flow angular variations for different Dean numbers are generally small and a point in every 5° seemed to be sufficient.

6. Results and discussion

For flows in a helical pipe there are two parameters ϵ and λ in addition to the Dean number. This can result in a large number of combinations. However, it appears that the general characteristics of the flow for various Dean numbers in the range we have covered remain basically unchanged, except that the intensities are different. Thus, to eliminate repetition most of the calculated results that we present here are for $D = 2000$ with only a few remarks made on flows at other Dean numbers, although numerical computations were actually carried out in the whole range up to $D = 5000$.

In order to see what the effect of torsion on the secondary flow pattern, we present a case of tightly coiled pipe with $\epsilon = 0.5$ in figure 9. There are two plots in this figure to depict the secondary flow vectors: figure 9(*a*) is for a curved pipe, and figure 9(*b*) is for a helical pipe with $\lambda = 0.1$. The secondary flow pattern in the latter is highly asymmetric and much distorted compared with the symmetric pattern in figure 9(*a*). In particular, the upper vortex is squashed and becomes much smaller than the lower one, although the core regions for these two vortices remain approximately in the

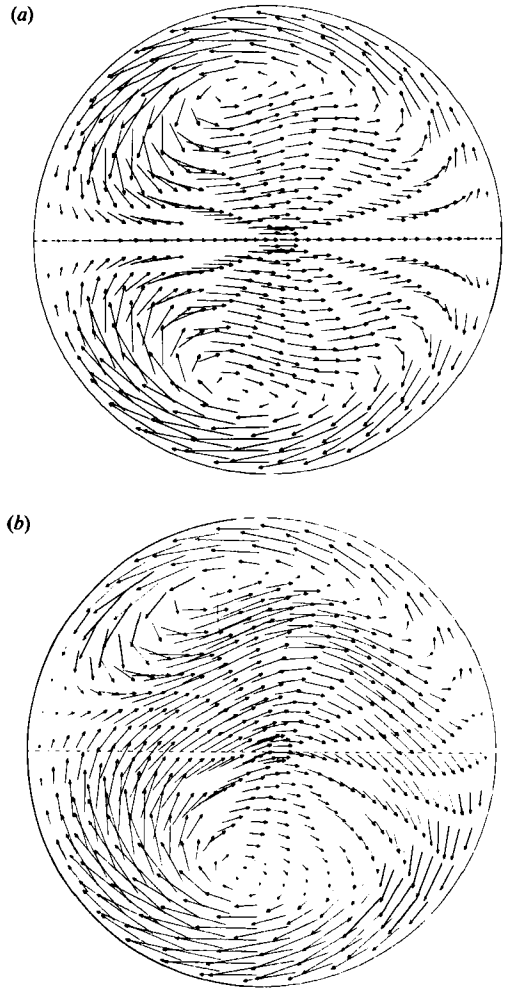

FIGURE 9. Vector plot of the secondary flow. (*a*) $D = 2000$, $\epsilon = 0.5$, $\lambda = 0$ (numerical solution). (*b*) $D = 2000$, $\epsilon = 0.5$, $\lambda = 0.1$ (numerical solution).

same locations as in figure 9(*a*). This suggests perhaps that the secondary flows in these two cases transport the fluid particles in a similar manner, which is reflected in the contour lines for the axial velocity components as illustrated in figure 10, which are seen to be similar. Consequently, the flux ratios are expected to be nearly equal in these two cases. This turns out to be true in general. A numerical example will be given later to substantiate this statement.

Before we proceed further, it is perhaps worth mentioning the meaning of the parameters. With reference to figure 1, the pitch is shown to be $2\pi b$, and the curvature κ and the torsion τ are defined as

$$\kappa = \frac{c}{b^2+c^2}, \quad \tau = \frac{b}{b^2+c^2}.$$

The corresponding dimensionless quantities are then

$$\epsilon = \kappa a = \frac{c}{b^2+c^2}a, \quad \lambda = \tau a = \frac{b}{b^2+c^2}a, \quad \lambda = \frac{b}{c}\epsilon.$$

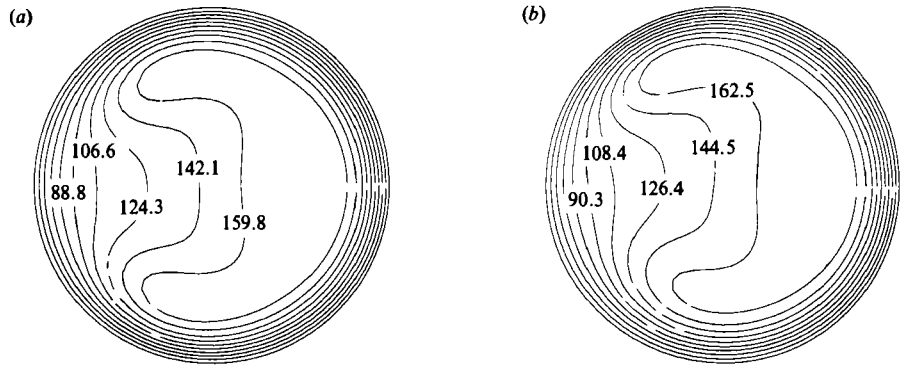

FIGURE 10. Contour lines of the streamwise velocity component corresponding to the two cases in figure 9. (*a*) $D = 2000$, $\epsilon = 0.5$, $\lambda = 0$ (numerical solution). (*b*) $D = 2000$, $\epsilon = 0.5$, $\lambda = 0.1$ (numerical solution).

It is seen that if $\epsilon = 0.5$ and $\lambda = 0.1$, the ratio $b/c = 0.2$, which represents a helical pipe of a fairly large pitch equal to approximately 1.2 times the radius of the pipe curvature. Thus, as the curvature decreases, the torsion must also decrease in order to maintain the ratio b/c constant.

Thus far the results obtained seem to indicate that the secondary flow patterns are controlled more by the ratio of λ to ϵ than by the individual parameters. To illustrate this, we include two secondary-flow vector plots in figure 11. Although ϵ and λ in figure 11 (*a*) are both smaller than those in figure 9 (*b*), the ratios λ/ϵ are comparable and the patterns are similar. (The vectors in figures 9 (*b*) and 11 (*a*) are adjusted by the same factor.) However, if ϵ is held constant and λ is reduced to 0.02, the ratio λ/ϵ becomes smaller, the flow pattern in figure 11 (*b*) appears to be nearly symmetric, and the effect of the torsion seems to have vanished. Although only a particular Dean number, $D = 2000$, is considered here, the finding of the diminishing effect of torsion as λ/ϵ becomes small, say less than 0.1, holds generally true at other Dean numbers as well.

In addition, two more cases for $\lambda/\epsilon = 0.1$, and $D = 2000$ were also considered: for $\epsilon = 0.3$, $\lambda = 0.03$ and for $\epsilon = 0.1$, $\lambda = 0.01$. The secondary-flow patterns are found to resemble closely those in figure 11 (*b*), although the counter-rotating vortices in the case of $\epsilon = 0.3$ are stronger than those in figure 11 (*b*), and those in the case of $\epsilon = 0.1$ are weaker. To avoid repetition the plots are not shown here.

In the first part of this paper for small Dean numbers with $\epsilon \ll 1$ and $\lambda \ll 1$, the controlling parameter, which determines whether a torsion can exert a $1\frac{1}{2}$-order effect, was the ratio $\lambda/(2\epsilon)^{\frac{1}{2}}$. However, if ϵ is not small (say, $0.4 \leqslant \epsilon$), nonlinear interactions become important, and a torsion with a relatively small $\lambda/(2\epsilon)^{\frac{1}{2}}$ ($=0.1$) can still cause a substantial distorsion in the secondary flows. Two examples have been given to demonstrate this circumstance: one is for a small Dean number in figure 7 and the other is in figure 9 (*b*). In order to see what a relatively large ratio can do to the flow field at $D = 2000$, we consider two additional cases and depict the results in figure 12. It turns out that the disposition of the vortices in the secondary flow in this case (figure 12*a*) is almost completely different from the usual symmetric shape. The lower vortex is so prevalent as to squeeze the upper vortex tightly in a narrow region with a poorly defined vortex core. This situation is almost similar to the single-vortex cell shown by Wang (1981).

At first glance it may appear that the secondary flow in figure 12 (*a*) is nearly all

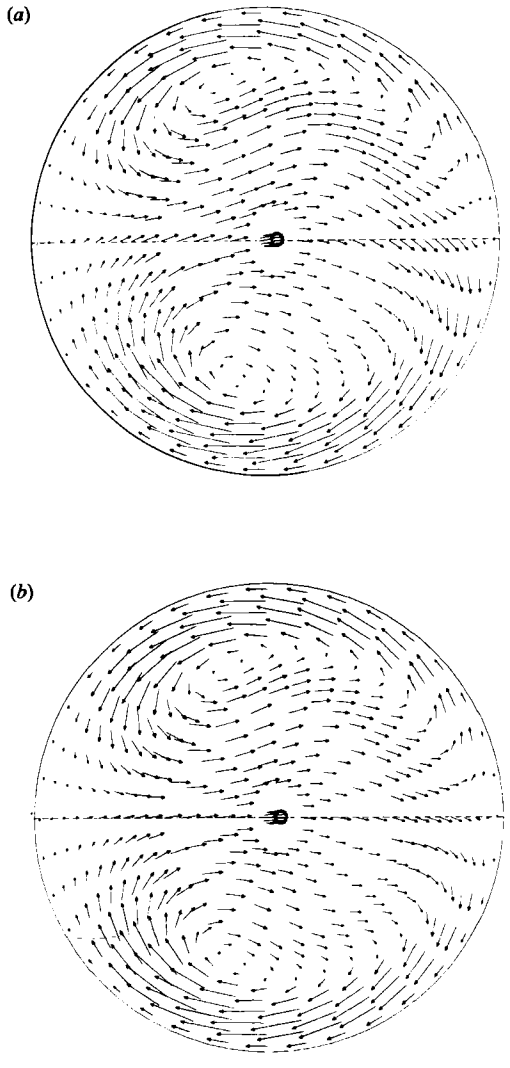

FIGURE 11. Vector plot of the secondary flow. (*a*) $D = 2000$, $\epsilon = 0.2$, $\lambda = 0.05$ (numerical solution). (*b*) $D = 2000$, $\epsilon = 0.2$, $\lambda = 0.02$ (numerical solution).

rotating in a clockwise direction and the total vorticity has a large negative value. This turned out to be not the case. In fact if the vorticity is integrated out through the computational domain, the total value is nearly zero, as it should be in accordance with Stokes's theorem.

Between the two counter-rotating vortices there should be a dividing streamline, though its position in the present example is not easily discernible. Nonetheless it is twisted, shifted upward, and situated mostly in the third quadrant. As a result the axial velocity contour lines are also distorted and shifted in the same direction. This is illustrated in figure 13(*a*).

Next we consider a case with $\lambda/(2\epsilon)^{\frac{1}{2}} = 0.25$, whose calculated results are displayed in figures 12(*b*) and 13(*b*). Although no special feature appears in these plots, they are included here for the purpose of filling the gap between $\lambda/(2\epsilon)^{\frac{1}{2}} = 0.5$, and $\lambda/(2\epsilon)^{\frac{1}{2}} \leqslant 0.1$, which are the values for the examples in figures 9–11.

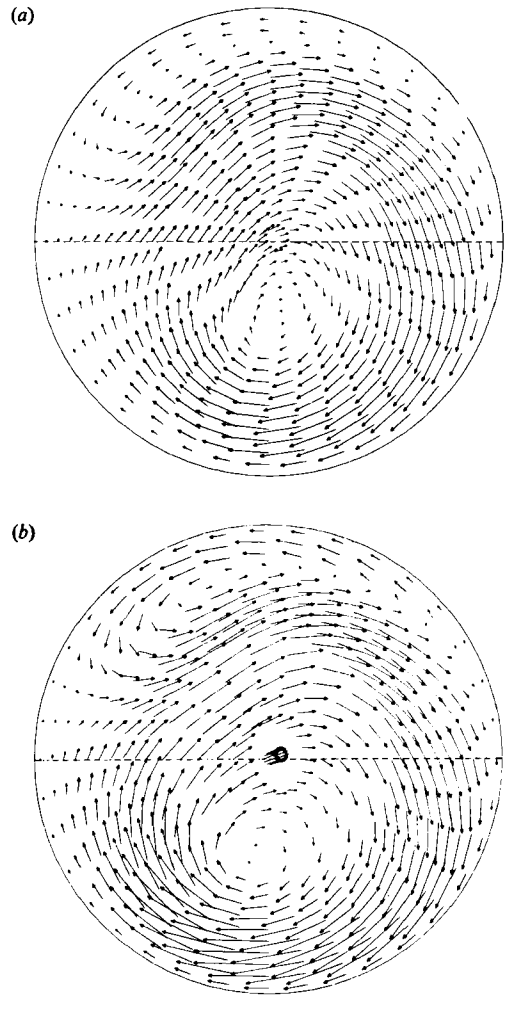

FIGURE 12. Vector plot of the secondary flow. (*a*) $D = 2000$, $\epsilon = 0.05$, $\lambda = 0.15811$ (numerical solution). (*b*) $D = 2000$, $\epsilon = 0.2$, $\lambda = 0.15811$ (numerical solution).

It is now fairly apparent from the axial velocity contour plots in various figures that these contour lines, though distorted, are not much different from the corresponding symmetric ones. As a result, the flux ratio in helical pipes is expected to be approximately equal to that in curved pipes at the same Dean number. However, it has been found that the former ratio is always slightly larger than the latter. This means that the flow resistance in a helical pipe is slightly smaller than the flow resistance in a curved pipe for the same Dean number. Although this property has been noted previously for small Dean numbers, it has not been shown for intermediate values. To this end we give two examples to demonstrate this circumstance:

$$\frac{Q}{Q_S} = 0.5186 \quad \text{at } D = 2000, \quad \epsilon = 0.2, \quad \lambda = 0 \quad \text{(curved pipe)},$$

$$\frac{Q}{Q_S} = 0.5192 \quad \text{at } D = 2000, \quad \epsilon = 0.2, \quad \lambda = 0.05 \quad \text{(helical pipe)}.$$

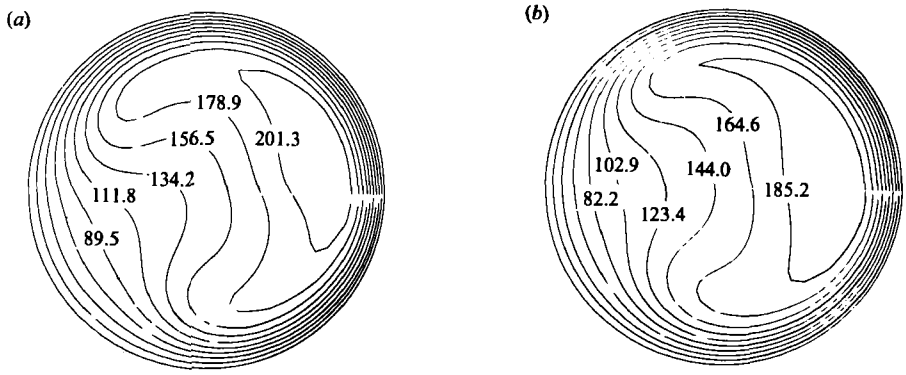

FIGURE 13. Contour lines of the streamwise velocity component corresponding to the two cases in figure 12. (*a*) $D = 2000$, $\epsilon = 0.05$, $\lambda = 0.15811$ (numerical solution). (*b*) $D = 2000$, $\epsilon = 0.2$, $\lambda = 0.15811$ (numerical solution).

The difference between these two ratios is rather small in this case. It will however, become slightly larger if the torsion or curvature is somewhat greater.

Dennis & Ng (1982) and others have discovered by means of the series truncation or other methods that there exists a second family of solutions in a curved pipe of $D > 956$, in which the secondary flow has a two-pair vortex structure instead of the usual one pair. It was thought that an additional parameter λ in the governing differential equations might make it possible to attain the dual solutions by the conventional finite-difference method without recourse to less familiar techniques. An attempt was therefore made to solve the existing system of finite-difference equations by giving initial conditions similar to the second family of solutions shown in Dennis & Ng's paper. However, all two-pair vortex solutions after a sufficient number of iterations always returned to the one-pair structure. Thus, it seems that the dual solutions, if existing in a helical pipe, may have to be obtained differently as for the case of curved pipes.

The author wishes to thank W. Y. Soh for many discussions about perturbations and curved pipes.

Appendix A

The equations of motion for a steady incompressible and fully developed flow in a helical pipe in dimensionless variables are

$$\frac{\partial}{\partial r}(ru)+\frac{\partial v}{\partial(\theta+\phi)} = -\epsilon\omega r[u\cos(\theta+\phi)-v\sin(\theta+\phi)]-\frac{\lambda}{(2\epsilon)^{\frac{1}{2}}}r\omega\frac{\partial w}{\partial(\theta+\phi)}, \quad \text{(A 1)}$$

$$\begin{aligned}&\frac{\partial^2 w}{\partial r^2}+\frac{1}{r}\frac{\partial w}{\partial r}+\frac{1}{r^2}\frac{\partial^2 w}{\partial(\theta+\phi)^2}-u\frac{\partial w}{\partial r}-\frac{v}{r}\frac{\partial w}{(\theta+\phi)}+\epsilon\omega\left[\cos(\theta+\phi)\frac{\partial w}{\partial r}-\frac{\sin(\theta+\phi)}{r}\frac{\partial w}{\partial(\theta+\phi)}\right]\\&\quad-\epsilon\omega[u\cos(\theta+\phi)-v\sin(\theta+\phi)]w-\epsilon^2\omega^2 w\\&=-\omega D-\lambda^2 r\omega^2 w\frac{\partial v}{\partial(\theta+\phi)}-\lambda(2\epsilon)^{\frac{1}{2}}\omega\left[ru\frac{\partial v}{\partial r}+\frac{1}{2}\frac{\partial v^2}{\partial(\theta+\phi)}+uv+\tfrac{1}{2}r\omega\sin(\theta+\phi)w^2\right]\\&\quad+\lambda(2\epsilon)^{\frac{1}{2}}\omega\left[r\frac{\partial\Omega}{\partial r}+\epsilon r\omega\Omega\cos(\theta+\phi)\right]\end{aligned}$$

$$-\lambda^2\omega^2\frac{\partial}{\partial(\theta+\phi)}\left[\frac{\partial w}{\partial(\theta+\phi)}-\epsilon r\omega w\sin(\theta+\phi)\right]$$

$$+\lambda^3(2\epsilon)^{\frac{1}{2}}r\omega^2\frac{\partial}{\partial(\theta+\phi)}\left(\omega\frac{\partial v}{\partial(\theta+\phi)}\right)$$

$$+\frac{\lambda}{(2\epsilon)^{\frac{1}{2}}}\omega\frac{\partial}{\partial(\theta+\phi)}(\tfrac{1}{2}w^2)-\lambda^2\omega\frac{\partial}{\partial(\theta+\phi)}\left(\omega\frac{\partial w}{\partial(\theta+\phi)}\right)$$

$$-\lambda\epsilon(2\epsilon)^{\frac{1}{2}}\omega^2\left[\cos(\theta+\phi)\frac{\partial u}{\partial(\theta+\phi)}-\sin(\theta+\phi)\frac{\partial v}{\partial(\theta+\phi)}\right]$$

$$-\lambda\epsilon(2\epsilon)^{\frac{1}{2}}\omega\frac{\partial}{\partial(\theta+\phi)}[\omega u\cos(\theta+\phi)-\omega v\sin(\theta+\phi)], \tag{A 2}$$

$$\frac{\partial^2\Omega}{\partial r^2}+\frac{1}{r}\frac{\partial\Omega}{\partial r}+\frac{1}{r^2}\frac{\partial^2\Omega}{\partial(\theta+\phi)^2}-\frac{1}{r}\left[\frac{\partial}{\partial r}(ru\Omega)+\frac{\partial}{\partial(\theta+\phi)}(v\Omega)\right]$$

$$-\epsilon\omega\left[\epsilon\omega\Omega+\frac{\sin(\theta+\phi)}{r}\frac{\partial\Omega}{\partial(\theta+\phi)}-\cos(\theta+\phi)\frac{\partial\Omega}{\partial r}\right]$$

$$=\omega w\left[\sin(\theta+\phi)\frac{\partial w}{\partial r}+\frac{\cos(\theta+\phi)}{r}\frac{\partial w}{\partial(\theta+\phi)}\right]+\frac{\lambda}{(2\epsilon)^{\frac{1}{2}}}\omega w\frac{\partial\Omega}{\partial(\theta+\phi)}$$

$$-\frac{\lambda}{(2\epsilon)^{\frac{1}{2}}}\left[\frac{1}{r}\frac{\partial(\omega w)}{\partial(\theta+\phi)}\frac{\partial u}{\partial(\theta+\phi)}-\frac{\partial(\omega w)}{\partial r}\frac{\partial v}{\partial(\theta+\phi)}\right]-\frac{\lambda}{(2\epsilon)^{\frac{1}{2}}}\epsilon\omega^2\left[\sin(\theta+\phi)\frac{\partial^2 w}{\partial r\,\partial(\theta+\phi)}\right.$$

$$\left.+\frac{\cos(\theta+\phi)}{r}\frac{\partial^2 w}{\partial(\theta+\phi)^2}\right]-\frac{\lambda}{(2\epsilon)^{\frac{1}{2}}}\epsilon\omega\frac{\partial}{\partial(\theta+\phi)}\left[\omega\sin(\theta+\phi)\frac{\partial w}{\partial r}+\frac{\omega\cos(\theta+\phi)}{r}\frac{\partial w}{\partial(\theta+\phi)}\right]$$

$$+\frac{\lambda}{(2\epsilon)^{\frac{1}{2}}}\epsilon^2\omega^3 w-\lambda^2\omega^2\left[\epsilon\omega r\sin(\theta+\phi)\frac{\partial\Omega}{\partial(\theta+\phi)}+\frac{\partial^2\Omega}{\partial(\theta+\phi)^2}\right]$$

$$+\lambda^2\epsilon\omega^3\left[\sin(\theta+\phi)\frac{\partial^2 u}{\partial(\theta+\phi)^2}+\cos(\theta+\phi)\frac{\partial v^2}{\partial(\theta+\phi)^2}\right]$$

$$+\lambda^2\epsilon\frac{\partial}{\partial(\theta+\phi)}\left[\omega^3\sin(\theta+\phi)\frac{\partial u}{\partial(\theta+\phi)}+\omega^3\cos(\theta+\phi)\frac{\partial v}{\partial(\theta+\phi)}\right]. \tag{A 3}$$

Here (A 1)–(A 3) are the continuity, axial momentum and vorticity transport equations respectively. D denotes the Dean number and

$$\omega=\frac{1}{1+\epsilon r\cos(\theta+\phi)}.$$

A modified stream function ψ is introduced:

$$w=\frac{\omega}{r}\frac{\partial\psi}{\partial(\theta+\phi)}-\frac{\lambda}{(2\epsilon)^{\frac{1}{2}}}\frac{\omega}{r}\int_0^r r\frac{\partial w}{\partial(\theta+\phi)}\mathrm{d}r,$$

$$v=-\omega\frac{\partial\psi}{\partial r},$$

to replace the continuity equation. With the aid of ψ and the definition of Ω (see (7)), we can express Ω in terms of ψ and w as follows:

$$\frac{\partial^2\psi}{\partial r^2}+\frac{1}{r}\frac{\partial\psi}{\partial r}+\frac{1}{r^2}\frac{\partial^2\psi}{\partial(\theta+\phi)^2}-\epsilon\omega\cos(\theta+\phi)\frac{\partial\psi}{\partial r}+\frac{1}{r}\epsilon\omega\sin(\theta+\phi)\frac{\partial\psi}{\partial(\theta+\phi)}$$
$$=-\frac{\Omega}{\omega}+\frac{\lambda}{(2\epsilon)^{\frac{1}{2}}}\frac{1}{r}\epsilon\omega\sin(\theta+\phi)\int_0^r r\frac{\partial w}{\partial(\theta+\phi)}\mathrm{d}r+\frac{\lambda}{(2\epsilon)^{\frac{1}{2}}}\frac{1}{r^2}\frac{\partial}{\partial(\theta+\phi)}\int_0^r r\frac{\partial w}{\partial(\theta+\phi)}\mathrm{d}r. \quad (A\,4)$$

This equation together with (A 2) and (A 3) are then the governing differential equations. The boundary conditions at $r=1$ for this system are

$$\psi=\frac{\lambda}{(2\epsilon)^{\frac{1}{2}}}\int_0^{\theta+\phi}\int_0^1 r\frac{\partial w}{\partial(\theta+\phi)}\mathrm{d}r\,\mathrm{d}(\theta+\phi),$$
$$\frac{\partial\psi}{\partial r}=w=0,$$
$$\Omega=\left(\frac{\partial v}{\partial r}\right)_{r=1},$$

where the quantity $\partial v/\partial r$ is evaluated at $r=1$ according to the three-point backward-difference formula after v is determined.

Appendix B

$$\psi_3=\frac{1}{320\times576}(1.3412\,r^2-3.0982\,r^4+\tfrac{9}{4}\,r^6-\tfrac{7}{12}\,r^8+\tfrac{5}{48}\,r^{10}-\tfrac{1}{70}\,r^{12}+\tfrac{1}{2016}\,r^{14})$$
$$\times\sin2\alpha+\frac{\beta}{320\times576}(1.9688\,r-0.6505\,r^3-0.1926\,r^4$$
$$+0.2006\,r^6-0.07407\,r^8+0.01667\,r^{10}-0.00221\,r^{12}+0.00012r^{14})$$
$$\times\cos\alpha+\frac{\beta}{320\times576}(0.69529\,r+2.4420\,r^3-4.675\,r^5+4.0559\,r^7-2.0986\,r^9$$
$$+0.65595\,r^{11}-0.11402\,r^{13}+0.00778\,r^{15})\sin\alpha,$$

$$w_3=\frac{1}{40\times(576)^2}(-3.67768+19\,r^2-\tfrac{331}{8}\,r^4+49.5\,r^6-\tfrac{569}{16}\,r^8$$
$$+15.7\,r^{10}-\tfrac{33}{8}\,r^{12}+\tfrac{4}{7}\,r^{14}-\tfrac{1}{32}\,r^{16})$$
$$+\frac{1}{40\times(576)^2}(25.8924r^2-\tfrac{2189}{35}\,r^4+\tfrac{3165}{56}\,r^6-24.7\,r^8+\tfrac{71}{12}\,r^{10}-\tfrac{87}{70}\,r^{12}+\tfrac{47}{280}\,r^{14}-\tfrac{4}{441}\,r^{16})$$
$$\times\cos2\alpha+\frac{\beta}{320\times576}(-0.4359\,r+1.07104\,r^3-1.1335\,r^5+0.7541\,r^7-0.3518\,r^9$$
$$+0.1195\,r^{11}-0.0266\,r^{13}+0.003403\,r^{15}-0.00017\,r^{17})$$
$$\times\cos\alpha+\frac{\beta}{320\times576}(0.3572\,r-0.2917\,r^3-0.7704\,r^4$$
$$+0.03289\,r^5+1.3579\,r^6-1.0321\,r^8$$
$$+0.4481\,r^{10}-0.11868\,r^{12}+0.01783\,r^{14}-0.00106\,r^{16})\sin\alpha.$$

REFERENCES

BERGER, S. A., TALBOT, L. & YAO, L. S. 1983 Flow in curved pipes. *Ann. Rev. Fluid Mech.* **15**, 461–512.

DEAN, W. R. 1928 The stream-line motion of fluid in a curved pipe. *Phil. Mag.* **5**, 673.

DENNIS, S. C. R. & NG, M. 1982 Dual solutions for steady laminar flow through a curved tube. *Q. J. Mech. Appl. Maths* **35**, 305.

GERMANO, M. 1982 On the effect of torsion on a helical pipe flow. *J. Fluid Mech.* **125**, 1.

HAMED, A. & ABDALLAH, S. 1979 Streamlike function: a new concept in flow problems formulation. *J. Aircraft* **16**, 801.

HAN, T., HUMPHREY, J. A. C. & LAUNDER, B. E. 1981 A comparison of hybrid and quadratic-upstream differencing in high Reynolds number elliptic flows. *Comput. Methods Appl. Mech. Engng* **29**, 81.

LARRAIN, J. & BONILLA, C. F. 1970 Theoretical analysis of pressure drop in the laminar flow of fluid in a coiled pipe. *Trans. Soc. Rheol.* **14**, 135.

LEONARD, B. P. 1979 A stable and accurate convective modelling procedure based on quadratic upstream interpolation. *Comput. Methods Appl. Mech. Engng* **19**, 59.

MANLAPAZ, R. L. & CHURCHILL, S. W. 1980 Fully developed laminar flow in a helically coiled tube of finite pitch. *Chem. Eng. Commun.* **7**, 57.

MCCONALOGUE, D. J. & SRIVASTAVA, R. S. 1968 Motion of a fluid in a curved tube. *Proc. R. Soc. Lond.* A **307**, 37.

MURATA, S., MIYAKE, Y., INABA, T. & OGAWA, H. 1981 Laminar flow in a helically coiled pipe. *Bull. JSME*, **24**, 355.

PATANKAR, S. V. 1980 *Numerical Heat Transfer and Fluid Flow*. Hemisphere.

SOH, W. Y. & BERGER, S. A. 1984 Laminar entrance flow in a curved pipe. *J. Fluid Mech.* **148**, 109.

TRUESDELL, L. C. & ADLER, R. J. 1970 Numerical treatment of fully developed laminar flow in helically coiled tubes. *AIChE J.* **16**, 1010.

VAN DYKE, M. 1978 Extended Stokes series: laminar flow through a loosely coiled pipe. *J. Fluid Mech.* **86**, 129.

WANG, C. Y. 1981 On the low-Reynolds-number flow in a helical pipe. *J. Fluid Mech.* **108**, 185.